Eur Biophys J (2010) 39:397–403
DOI 10.1007/s00249-009-0412-6

ORIGINAL PAPER

Investigation of β-carotene–gelatin composite particles with a multiwavelength UV/vis detector for the analytical ultracentrifuge

Engin Karabudak · Wendel Wohlleben · Helmut Cölfen

Received: 14 November 2008 / Revised: 23 January 2009 / Accepted: 29 January 2009 / Published online: 26 February 2009

Abstract A multiwavelength UV/vis detector for the analytical ultracentrifuge (MWL-AUC) has been developed recently. In this work, β-carotene–gelatin composite particles are investigated with MWL-AUC. Band centrifugation with a Vinograd cell is used to ensure maximum sample separation. Spectral changes of the system are observed in dependence of the sedimentation coefficient and are attributed to a previously unknown inhomogeneity of the β-carotene chemical composition with both H- and J-aggregates coexisting in a mixture. In addition, our data suggest that pure H- and J-aggregates exist in a particle while their relative concentrations in a mixture determine the color characteristics of the sample. The unique abilities and properties of MWL-AUC include sedimentation coefficient distributions for all possible wavelengths, full UV/vis spectra of each different species in the mixture and 3D movies of the sedimentation process. These properties significantly extend the scope of the analytical ultracentrifuge technique and show that complex biopolymer multicomponent mixtures can be resolved into their individual species.

AUC&HYDRO 2008—Contributions from 17th International Symposium on Analytical Ultracentrifugation and Hydrodynamics, Newcastle, UK, 11–12 September 2008.

Electronic supplementary material The online version of this article (doi:10.1007/s00249-009-0412-6) contains supplementary material, which is available to authorized users.

E. Karabudak · H. Cölfen (✉)
Colloid Chemistry, Max Planck Institute of Colloids and Interfaces, Research Campus Golm, 14424 Potsdam, Germany
e-mail: Coelfen@mpikg.mpg.de

W. Wohlleben
Polymer Physics Research, BASF SE, 67056 Ludwigshafen, Germany

Introduction

Analytical Ultracentrifugation is an analytical absolute technique applying centrifugal force to fractionate the sample and optical detection systems to detect the concentration distribution of the sample inside the ultracentrifuge cell. These experiments yield a number of important physico-chemical quantities of the sample like size, shape, density, molar mass, sedimentation and diffusion coefficient, interaction constants and stoichiometry etc. and many of them in form of distributions. However, often the available information depends on the applied optical detection system. Optical systems that have been constructed are UV/vis absorption, Rayleigh interference, Schlieren and the Lavrenko Optics (Lavrenko et al. 1999; Lloyd 1974). Development of new optical detection systems can expand the possible use of AUC for different types of samples. Size distributions can be determined with Turbidity optics (Mächtle 1992; Müller 1989; Scholtan and Lange 1972). Fluorescence optics has expanded the use for extremely diluted labeled samples even in presence of other solutes at a much higher concentration (MacGregor et al. 2004; Schmidt and Riesner 1992). The only commercially available machine at the moment is the Beckman XL-I which is equipped with a UV/vis absorption optics and Rayleigh interference optics (Giebeler 1992). Recently, the UV/vis absorption detection was significantly improved by the development of a multiwavelength UV/vis absorption detector (MWL-AUC). By essentially replacing the monochromator with a spectrograph, the MWL-AUC delivers an entire UV/vis spectrum for each radial point instead of a single wavelength reading (Bhattacharyya et al. 2006; Strauss et al. 2008). This technology has a number of advantages over the commercial absorption optics detecting at a single wavelength with time-consuming wavelength

scanning, thus excluding the study of all fast processes, Obtaining full UV/vis spectra at each point in the ultracentrifuge cell rather than a radial concentration profile at a single wavelength can give much more structural information about the sample, allows for averaging and can even decrease the experimental time when modern fast CCD based spectrometers are used (Bhattacharyya et al. 2006; Strauss et al. 2008). Successful optical, mechanical, radial scan, linearity and noise tests of the MWL detector have been published recently (Strauss et al. 2008).

Combined with the fractionating power of the AUC, application of the MWL detector with its additional structural and/or compositional information on light absorbing samples can yield distributions of the individual components in complex mixtures with respect to composition and size/density related to different chromophores. This can start with relatively straightforward issues like sample homogeneity and purity but can then get increasingly complex in case of composite and/or interacting samples. Especially for such complex samples MWL-AUC has a huge potential, as spectral discrimination can synergistically enhance the hydrodynamic resolution (Balbo et al. 2005). This is also an important issue for any colored industrial product composed of at least two components which at least slightly differ in their UV/vis spectra. In this work, we will show the capabilities of MWL-AUC for the analysis of an industrial composite sample of β-carotene and gelatin. This system was investigated before with X-ray scattering, UV/vis absorption spectroscopy, FOQELS (Fiber-optic quasi-elastic light scattering), microelectrophoresis and on basis of these results, a core-shell structure was presented (Auweter et al. 1999), as shown in Fig. 2. The core structure with 120 nm diameter consists of partially crystallized, partially amorphous β-carotene as active ingredient. The shell structure consists of gelatin, functioning as bio-degradable protection colloid. This hybrid structure self-assembles in a carefully tuned co-precipitation of gelatin (from an aqueous solution) and the active ingredient (from a lipophilic solvent). Such particulate formulations can transport an active ingredient that is not water soluble across an aqueous phase with high bioavailability, in this case provitamin A. These particles are not persistent, but disassemble and get digested quickly in biological media.

There are two forms of hydrosol that are explained in Auweter et al. (1999). β-carotenes can precipitate as H-aggregate or J-aggregate; the two morphologies do not interconvert and are regarded to be kinetically stable over years. The H-aggregate is observed in precipitation of dilute solutions (0.3 weight%) whereas the J-aggregate is observed at higher concentration (1.0 weight%). Auweter et al. (1999) calculated a 40 nm hypsochromic shift observed for an H-aggregate and a bathochromic shift in J-aggregates. This results in a significant color change from yellow to red of the product depending on the precipitation conditions and hybrid particle size (Figs. 1, 2). This color change is the basis for the industrial application of the β-carotenes as pigments for food applications.

Not only the purity of the sample concerning the color characteristics (brilliance of color due to steep absorbance profiles) or sample homogeneity (different species or unbound gelatin) is of interest for the industrial application but furthermore any possible transitions between different structures. This is a problem which can be advantageously solved in a single MWL-AUC experiment, which we will describe in this work.

Materials and methods

The β-carotene product was obtained in powder form as a laboratory sample from BASF SE, Ludwigshafen. An aqueous dispersion in water was prepared with a concentration of 0.05 g/l. The UV/vis spectrum of the dispersion and of the free gelatin is shown in Fig. 1.

Multi-wavelength analytical ultracentrifugation (MWL-AUC)

A Multiwavelength AUC as described in Bhattacharyya et al. (2006) and Strauss et al. (2008) was used at 25°C. We have applied a band centrifugation experiment using a Vinograd cell. In contrast to conventional sedimentation velocity experiments, where the sample between boundary and bottom of the cell is only diluted by radial dilution, the sample in band centrifugation is diluted additionally by fractionation in the pure solvent. The reservoir is filled with a

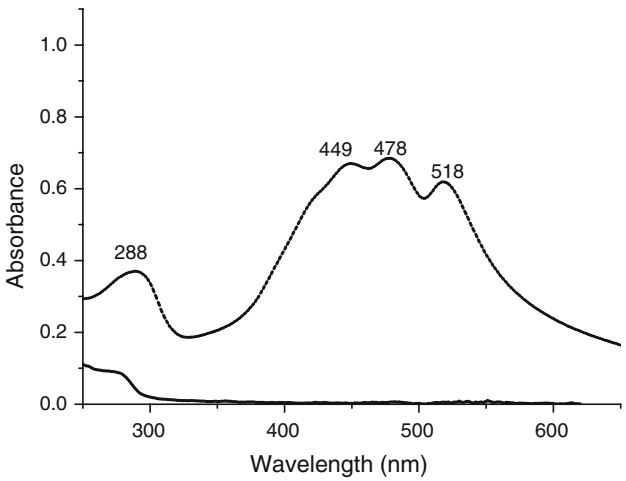

Fig. 1 *Dashed line* UV/vis spectrum of the core-shell β-carotene/gelatin sample with 0.05 g/l concentration; *solid line* UV/vis spectrum of gelatin at 1 g/l

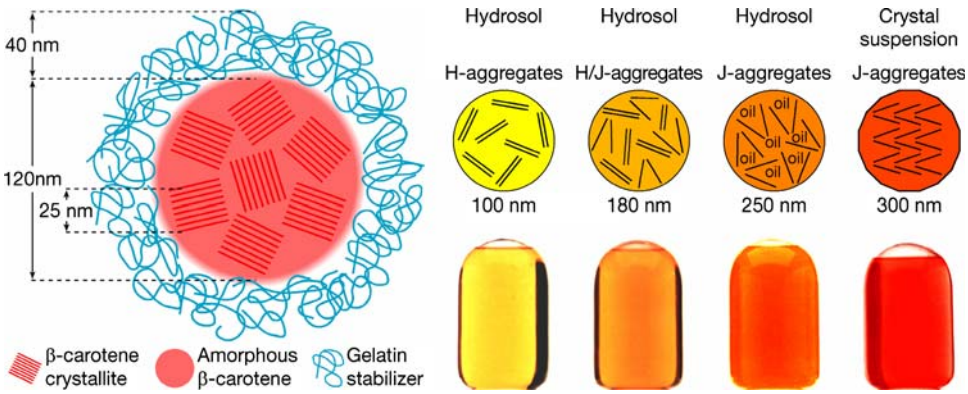

Fig. 2 *Left side* Assumed structure of the β-carotene microparticle system (Auweter et al. 1999), *right side* color change of β-carotene/gelatin microparticles due to particle size and structure

small amount of concentrated sample. Column and sample sectors are filled with D_2O with a density which is higher than that of the sample solution and lower than the density of the dispersed solute. We have prepared a 20 g/l solution and deposited 15 µl of the solution into the cell reservoir. After preliminary experiments, this concentration was chosen to ensure that the individual components of the mixture are detected in as many as possible scans with OD's < 1.4 in the experiment without too much dilution which causes noisy data.

After cell assembly, the AUC was accelerated to 5,000 rpm for 3 min to transfer the sample in the reservoir via capillaries to overlay the D_2O column. Afterwards, the speed was increased to 55,000 rpm. Forty scans were taken with a time interval of 90 s and a radial step size of 50 µm to observe the full sedimentation of the sample. The selected wavelength range was 250–750 nm. In the prototype setup, we apply the spectrum acquired for an empty cell as a reference for the calculation of the absorption leading to a baseline offset of 0.05 OD (see Fig. 3i) After the experiment, while cleaning the cell, we saw some precipitate in the cell reservoir. Thus, not all particles were transferred to the sample column, but some big particles remained in the reservoir as they already must have completely sedimented upon speeding up the rotor to 5,000 rpm.

Each of the 40 scans produces a 3-dimensional graph. We have radial position as x-dimension, wavelength as y-dimension and absorbance as z-dimension. In the present contribution, we will perform a semi-quantitative evaluation based on simple model-free transformations of the data without any prior knowledge.

For evaluation, we have converted the radial position (r) to the sedimentation coefficient s by using Eq. 1. In Eq. 1, r_m is the radial position of the meniscus and $\omega^2 t$ is the run time integral.

$$s = \frac{\ln(r/r_m)}{\omega^2 t} \quad (1)$$

The 3D absorption dataset can now be projected either onto the wavelength or sedimentation coefficient axis to better visualize the spectral changes with different sedimentation coefficients or sedimentation coefficient distributions at different wavelengths.

Results and discussion

In principle, the entire dataset can be evaluated globally, and efforts are underway to incorporate such routine into the Ultrascan evaluation software package (Demeler 2005). However, even then we are confronted with a confounded polydispersity of both optical and colloidal/hydrodynamic properties. In the left side of Fig. 2, the assumed core-shell structure of a β-carotene microparticle is shown (Auweter et al. 1999). Such a complex hybrid particle exhibits several levels of polydispersity, which impact the distribution of sedimentation coefficients observed in an AUC. They are for example:

1. diameter of the inner core;
2. chemical composition, esp. oil content, of the inner core;
3. concentration of the adsorbed protection colloid (gelatin);
4. degree of swelling of the gelatin.

Parameters 1 and 2 determine the optical properties and bioavailability that are decisive for the commercial application profile. For smallest particle sizes, β-carotene is an H-aggregate while for the biggest particle sizes β-carotene forms J-aggregates. Intermediate particle sizes are assumed to integrate H- and J-aggregates in differing ratio (Auweter et al. 1999). Parameters 3 and 4 determine the thickness of the protection colloid layer, which is typically 40 nm in pure water. The buoyant density of gelatin is rather high (above 1.3 g/cm^3), and cannot be matched with a non-interfering solvent such as heavy water.

All parameters 1–4 enter into the calculation of the effective density and the hydrodynamic diameter of the hybrid particle. The frictional force under sedimentation depends on the ion concentration and pH because the

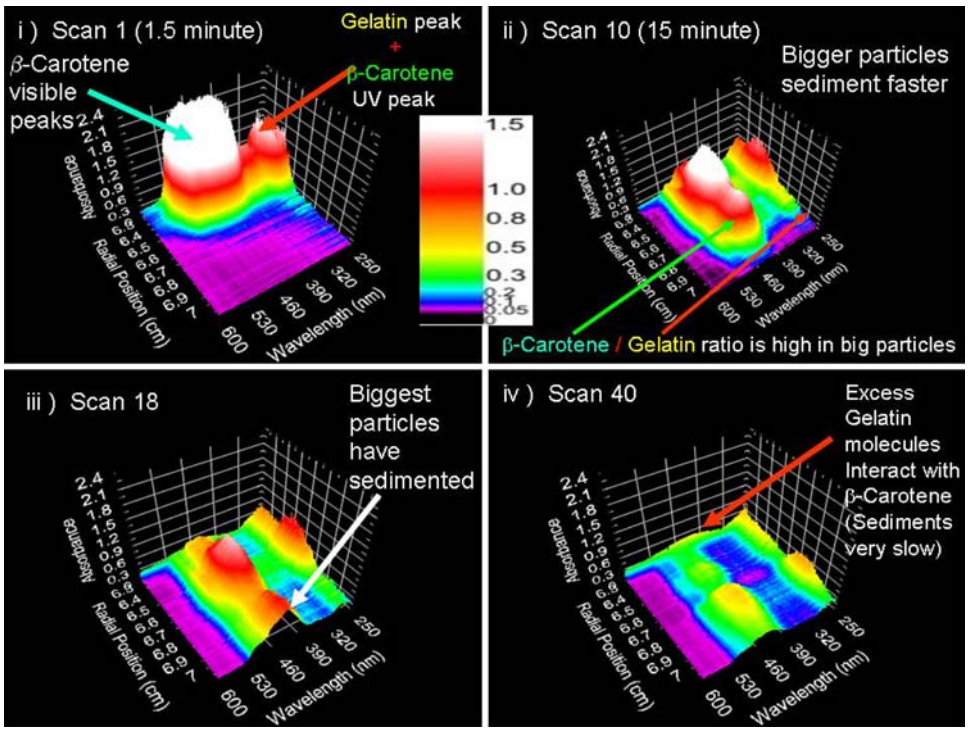

Fig. 3 Three-dimensional plots of the raw data from a band sedimentation experiment with β-carotene detected with the MWL detector. The axes are wavelength, absorbance and radial position. *i* Scan 1 (1.5 min); *ii* Scan 10 (15 min); *iii* Scan 18 (27 min); *iv* Scan 40 (60 min)

gelatin may collapse or swell thus changing the effective frictional forces (and thus changing the observable sedimentation constant) although the chemical composition and buoyant density, which in principle could be measured in a Krattky gauge or density gradient, stay the same. The swelling of the gelatin corona alone impedes an exact conversion from measured sedimentation constants to hydrodynamic diameters. Considering that also parameters 1 and 2 contribute to the polydispersity in the observable distribution of sedimentation coefficients, we decided to limit ourselves to a conservative evaluation on the level of sedimentation fractions, not sizes.

We now discuss the optical properties that result from the specific colloidal microstructures as discussed above. Due to different preparation conditions, the morphology of the β-carotene core changes. H- and J-aggregates have different UV/vis spectra, shown as visual impression on the right side of Fig. 2. Figure 1 dot line curve shows the UV/vis spectrum of 0.05 g/l product without any ultracentrifugation. Four peaks at 288, 449, 478 and 518 nm can be seen. The three peaks in the visible can be attributed to the $1A_g^-$ (S0)–$1B_u^+$ (S2) transition with the vibrational progression 2–0, 1–0, 0–0 of the C–C stretch vibration along the alternatingly double bonded electronically conjugated backbone of the carotenoid (Polivka and Sundstrom 2004).The UV peak partially can be attributed also to the carotenoid transition $1A_g^-$–$1A_g^+$, which is forbidden by symmetry, but becomes allowed in the crystalline assembly. The spectrum of the composite particle indicates the β-carotene J-aggregate (Auweter et al. 1999). Figure 1 solid curve shows the pure gelatin spectrum for 1 g/l. It can be seen that gelatin only contributes to the UV region of the spectra below 280 nm. However, the contribution of gelatin is vanishing compared to the three times stronger absorption of the composite sample at 20 times lower overall concentration. Another component that presumably contributes to the UV absorption is the ascorbylpalmitat dispersant that is added during the co-precipitation.

Figure 3 shows four of the 40 experimental scans. If we put all these 40 scans in sequence, we can form a 3D movie of the sedimentation process. This movie is available as supplementary information. Figure 3.1 shows scan 1 where particles just have been transferred from the reservoir to the sample column. The baseline offset is 0.05 (purple) due to the absorption calculation with an empty cell as reference. We see two main peaks. The peak in the visible region is assigned to β-carotene. In the UV range, there is an overlay of two peaks, one is the UV peak of β-carotene (see Fig. 2) and the other is the UV signal of gelatin. After 15 min of sedimentation, fractionation of the sample is obvious and the first sedimentation fraction proceeds to the bottom of the cell. Scan 10 (15 min) is the last scan where the entire particle range can be seen before the first particles reach the bottom. If we compare the height of the peak in the UV and visible region at different radial positions, the ratio changes. For the faster sedimenting particles, the ratio of β-carotene to gelatin is higher. This is the first important result, demonstrating that the sample is not homogenous. Instead, the particles change their colloidal properties in correlation with the optical properties. The observed effect

can be explained by a higher content of stabilizing agent that induces smaller particle sizes. Note that the shape of the peak at 288 nm (Fig. 1) does not exactly match the gelatin absorption and that the expected contribution of gelatin is weak at the applied concentrations, hinting at a combined action of both gelatin and the ascorbylpalmitat added during the co-precipitation in particle synthesis. The third part of Fig. 3 shows the scan after 27 min. Here, the fastest particles have sedimented already. In the fourth part of Fig. 3, we see the last fraction that remained after 60 min of sedimentation, which is mainly composed of gelatin. However, some β-carotene absorption is still visible, which seems to be solubilized in small amount by the excess gelatin or excess ascorbylpalmitat. We do not detect free gelatin in the analysis. In an independent experiment we measured the characteristic sedimentation behavior of gelatin with the interference optics of the Beckman XLI AUC at 44,000 rpm. We found a sedimentation constant distribution from 2 to 10 Sved. This confirms our assignment that the last fraction cannot be pure gelatin.

To summarize the global evaluation, Fig. 3 demonstrates the power of MWL-AUC. We can differentiate particles, observe the full UV/vis spectra of the particles and can already draw conclusions about the different components in the complex sample mixture without any further evaluation, as the *Y*-axis shows the full UV/vis wavelength range. This is a key feature of MWL-AUC. Such analysis was impossible in analytical ultracentrifugation experiments before.

We can also use projections of the data onto individual axes and proceed thus to a more quantitative evaluation. In order to calculate the full s-distribution of all particles, we have selected scan 10 for all further evaluation as this scan shows fractionation of the mixture while no particles are yet lost due to complete sedimentation. More information is potentially available with a global evaluation of the entire dataset. In Fig. 4, the s-distribution of the particles is shown for 5 different representative wavelengths out of 330 (250–750 nm with a wavelength resolution of 1.5 nm). We have selected the wavelengths according to the peaks of the β-carotene microparticles: 260, 280, 450, 480 and 520 nm in Fig. 1.

The s-distribution is obviously very broad. Due to the chemical heterogeneity of the particles and the resulting density distribution, it is not possible to convert the sedimentation coefficient to the particle size. However, all important sample characteristics can be discussed for the s-distributions. From Fig. 4, we conclude that there are at least three fractions in the sample: small hybrid particles with $s < 25$ S, a main fraction around 100 S and larger particles around 200 S. Their absorption spectra (and chemical composition) are clearly different as can be seen in Fig. 5.

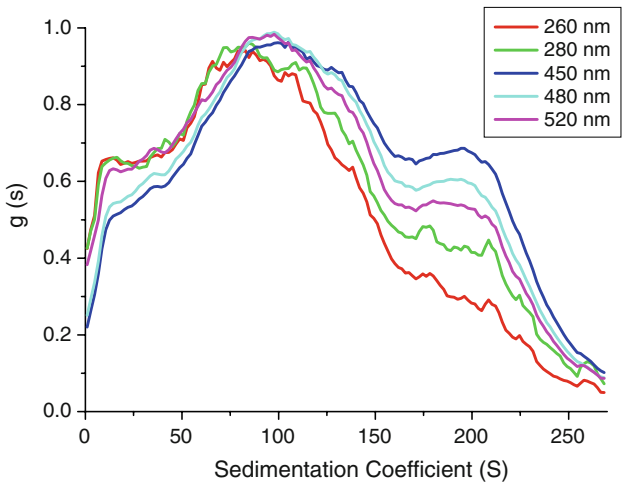

Fig. 4 Sedimentation coefficient distributions at different wavelengths

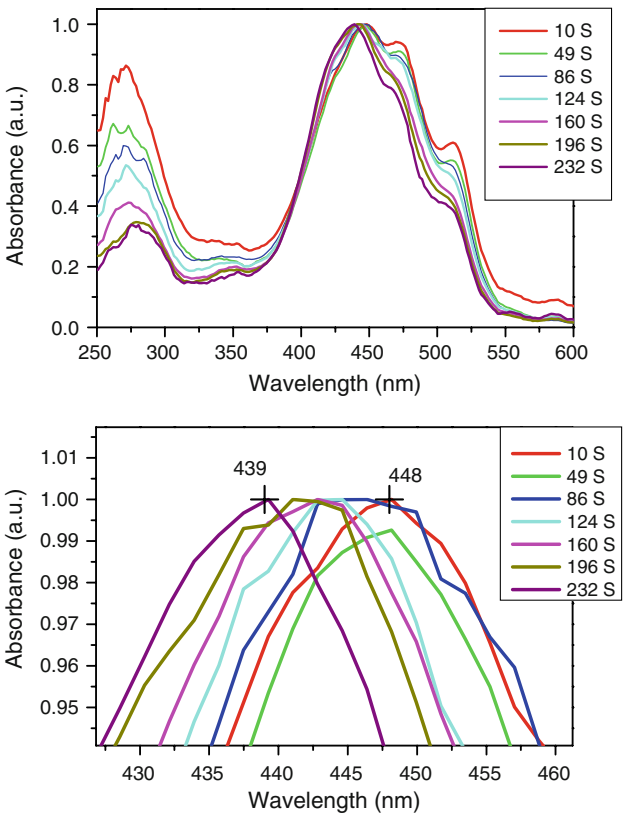

Fig. 5 *Top* Normalized UV/vis spectra of particles with different sedimentation coefficients, *bottom* zoom the range around 450 nm and peak positions of 10.6 S (448 nm) up to 232 S (439 nm)

In Fig. 5, seven representative UV/vis spectra are shown. The spectra agree well with those of pure H-aggregates (Auweter et al. 1999). However, the original sample contained J-aggregates too (Fig. 1, dashed line). We believe that the J-aggregates were already precipitated before the first scan in the AUC cell was taken. Indeed

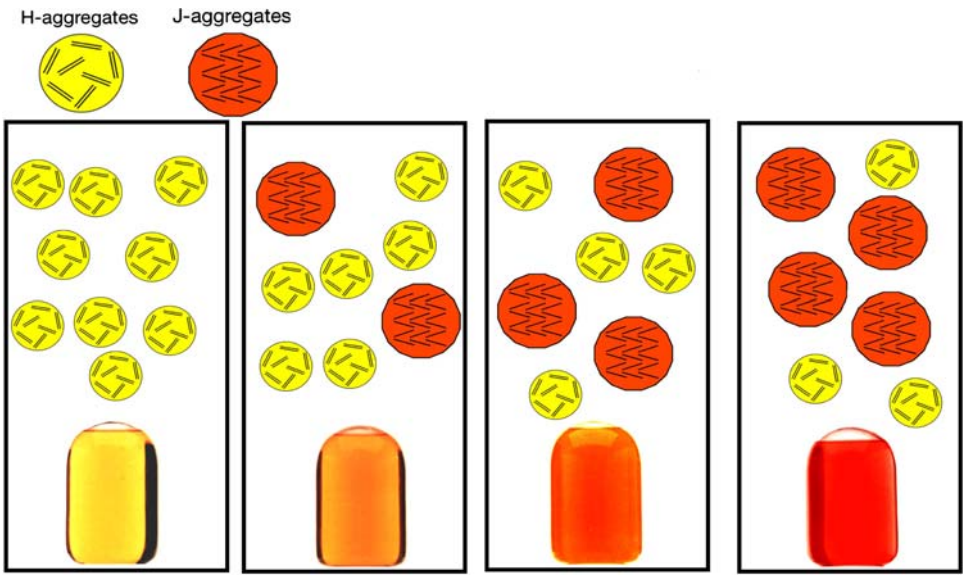

Fig. 6 Ad hoc structural model of the β-carotene microparticle system on basis of the presented AUC results. The different color of the samples does not originate from the intraparticular coexistence of H- and J-aggregates as assumed before (Fig. 2) (Auweter et al. 1999) but instead separate particles contain pure H- or J-aggregates and the concentration ratio between these particles determines the colour of the final sample. Note the difference to Fig. 2

precipitation of particulate material inside the reservoir of the vinograd cell was observed visually after cell disassembly following the experiment. However, irrespective of the actual nature of the particulate material that remained in the Vinograd cell reservoir, the result stands for itself that the coloristic polydispersity (Fig. 1) is not due to an intra-particle but inter-particle distribution of morphologies (Fig. 6). This result is contrary to the previous assumption that is sketched in Fig. 2, where H/J-aggregates would coexist in the particles.

The peak around 520 nm slightly shifts to lower wavelength with increasing sedimentation coefficient and the peak height also decreases. The same is true for the peak at 480 nm. Therefore, this excitation of β-carotene microparticles decreases with increasing sedimentation coefficient. For the peak at 450 nm, only the spectral shift to lower wavelength is observed with increasing sedimentation coefficient. The effects of this inhomogeneity were not known before in such detail. We suspect that the displacement of the electronic potential energy surfaces changes, such that the Frank–Condon—factors change for the vibrational progression, due to the changing incorporation of the chromophore into the partially crystalline assembly.

As discussed above, an overlay of the signal from β-carotene, gelatin and the ascorbylpalmitat is observed in the UV region. In this range, a shift of the peak maximum to higher wavelength with increasing sedimentation coefficient is detected. In addition, a drastic decrease of the peak height relative to the 450 nm peak is observed with increasing sedimentation coefficient. The particles that sediment slower show stronger UV absorption, which we attribute to a higher content of ascorbylpalmitat, and hence smaller particle diameters due to the formation process in co-precipitation Auweter et al. 1999). To our knowledge, it is the first time that relatively small steps of spectral shift among an H-aggregate are shown for composite particles. All of the 200 different detected spectra follow the same trend. Although the spectral changes appear to be continuous, that does not exclude defined and different spectra for different particle populations as the detected raw signals are those of a sample band, which is broadened by polydispersity in size, composition and diffusional broadening.

Conclusion

Industrial β-carotene–gelatin composite particles are a highly heterogeneous system—both in particle size and chemical composition. Fractionation of this mixture in MWL-AUC allows to resolve individual components in the mixture and detect compositional changes in an experiment, which takes only 1 h. This proves the power of MWL-AUC as a direct technique that can differentiate particles with respect to size and UV/vis spectra. Although our current analysis does not allow to unambiguously assign the spectra to defined particles as the particle density, swelling, composition and size maybe varying simultaneously, the presented multiwavelength analysis allows insights into this complex system, which were not possible before by other techniques. We do not further evaluate the directly experimentally determined sedimentation coefficients as for our sample, in addition to the above mentioned polydispersity, pH effects as well as charge interactions between the colloids also have to be taken into account.

Despite these restrictions, we have shown the existence of H-aggregates inside a sample that was previously known as J-aggregate and have detected spectral changes of

different H-aggregate populations as well as changes in the electronic potential energy surfaces of different hybrid particles. We restricted ourselves to a semi-quantitative evaluation based on simple model-free transformations of the data of 1 out of 40 scans without any prior knowledge. Clearly, even richer phenomena can potentially be discovered with a global evaluation of the entire dataset.

Acknowledgments We thank the BASF SE and the Max-Planck society for financial support of the Multiwavelength Detector project.

References

Auweter H, Haberkorn H, Heckmann W, Horn D, Luddecke E, Rieger J, Weiss H (1999) Supramolecular structure of precipitated nanosize beta-carotene particles. Angew Chem Int Ed 38:2188–2191. doi:10.1002/(SICI)1521-3773(19990802)38:15<2188::AID-ANIE2188>3.0.CO;2-#

Balbo A, Minor KH, Velikovsky CA, Mariuzza RA, Peterson CB, Schuck P (2005) Studying multiprotein complexes by multisignal sedimentation velocity analytical ultracentrifugation. Proc Natl Acad Sci USA 102:81–86. doi:10.1073/pnas.0408399102

Bhattacharyya SK, Maciejewska P, Börger L, Stadler M, Gülsün AM, Cicek HB, Cölfen H (2006) Development of a fast fiber based UV-Vis multiwavelength detector for an ultracentrifuge. Prog Colloid Polym Sci 131:9–22. doi:10.1007/2882_002

Demeler B (2005) ULTRASCAN: a comprehensive data analysis software package for analytical ultracentrifugation experiments. In: Scott DJ, Harding SE, Rowe AJ (eds) Modern analytical ultracentrifugation: techniques and methods, pp 210–229

Giebeler R (1992) The optima XL-A: a new analytical ultracentrifuge with a novel precision absorption optical system. In: Harding SE, Rowe AJ, Horton J (eds) Analytical ultracentrifugation in biochemistry and polymer science. Royal Society of Chemistry, Cambridge, pp 16–25

Lavrenko P, Lavrenko V, Tsvetkov V (1999) Shift interferometry in analytical ultracentrifugation of polymer solutions. Prog Colloid Polym Sci 113:14–22. doi:10.1007/3-540-48703-4_3

Lloyd P (1974) Optical methods in ultracentrifuge, electrophoresis and diffusion: with a guide to interpretation of records. Clarendon, Oxford

MacGregor IK, Anderson AL, Laue TM (2004) Fluorescence detection for the XLI analytical ultracentrifuge. Biophys Chem 108:165–185. doi:10.1016/j.bpc.2003.10.018

Mächtle W (1992) Analysis of polymer dispersions with an eightcell-auc-multiplexer: high resolution particle size distributions and density gradient techniques. In: Harding SE, Rowe AJ, Horton J (eds) Analytical ultracentrifugation in biochemistry and polymer science. Royal Society of Chemistry, Cambridge, pp 147–175

Müller HG (1989) Automated determination of particle-size distributions of dispersions by analytical ultracentrifugation. Colloid Polym Sci 267:1113–1116. doi:10.1007/BF01496933

Polivka T, Sundstrom V (2004) Ultrafast dynamics of carotenoid excited states—from solution to natural and artificial systems. Chem Rev 104:2021–2071. doi:10.1021/cr020674n

Schmidt B, Riesner B (1992) A fluorescence detection system for the analytical ultracentrifuge and its applicaton to proteins, nucleic acids, viroids and viruses. In: Harding SE, Rowe AJ, Horton J (eds) Analytical ultracentrifugation in biochemistry and polymer science. Royal Society of Chemistry, Cambridge, pp 176–207

Scholtan W, Lange H (1972) Bestimmung der Teilchengrößenverteilung von Latices mit der Ultrazentrifuge. Colloid Polym Sci 250:782–796. doi:10.1007/BF01498571

Strauss HM, Karabudak E, Bhattacharyya S, Kretzschmar A, Wohlleben W, Cölfen H (2008) Performance of a fast fiber based UV/vis multiwavelength detector for the analytical ultracentrifuge. Colloid Polym Sci 286:121–128. doi:10.1007/s00396-007-1815-5